24 March 1995

ELSEVIER

Chemical Physics Letters 235 (1995) 175–182

CHEMICAL PHYSICS LETTERS

Inelastic scattering of NO($^2\Pi$) with atomic and molecular colliders. Rotational and fine-structure excitations

C.R. Bieler, A. Sanov, H. Reisler

Department of Chemistry, University of Southern California, Los Angeles, CA 90089-0482, USA

Received 16 December 1994; in final form 11 January 1995

Abstract

The inelastic collisions of NO ($T_{rot} \leqslant 5$ K) with Ar, Xe, CO, N_2, O_2, N_2O and CO_2 were studied in molecular beams at center-of-mass collision energies 750–2500 cm^{-1}. Rotational, Λ-doublet and spin–orbit distributions of scattered NO($^2\Pi_{1/2,3/2}$) were determined. In all the scattering experiments (with the possible exception of Ar) no preferences were observed in the Λ-doublet populations. The rotational distributions all appear Boltzmann-like, with somewhat different rotational temperatures. The populations of the $^2\Pi_{1/2}$ and $^2\Pi_{3/2}$ spin–orbit states depend on the nature of the collider, but do not show any clear relationship with the extent of rotational excitation. No evidence of long-range attractive interactions is revealed in any of the systems studied.

1. Introduction

Inelastic collisions of open-shell molecules have attracted considerable experimental and theoretical interest partly because the possibility of attractive interactions makes their studies relevant to unimolecular and bimolecular reactions [1]. At the energies relevant to most chemical reactions, excitations of the rotational and fine-structure degrees of freedom are the most common outcomes. For highly averaged ensembles, these excitations often obey simple energy gap laws [2–4]; however, when the experiments are carried out with initial and final state selection, state-specific effects are often observed, revealing details of the potential energy surfaces (PES) governing the collisional interaction [5–8].

Previous work on the inelastic collisions of diatomic molecules with noble gases (e.g., Ar, He) has shown that when the molecule is in a $^2\Pi$ state (e.g., NO, OH, or CH in their ground electronic states), the cylindrical degeneracy is lifted by the approaching collider resulting in two PESs corresponding to wavefunctions of A′ and A″ reflection symmetry [9–12]. The final fine-structure and rotational distributions depend sensitively on these PESs and the interference between the wavefunctions in the exit channel [11,13–16]. This can sometimes result in nonstatistical Λ-doublet distributions in the diatomic molecule, even when in the initial state the two components are equally populated [17,18]. In the inelastic scattering of NO with Ar, for which a wealth of experimental and theoretical information is available [12,15,19–22], it was shown that for low rotational excitations (i.e. when the excited NO is described by Hund's case (a) wavefunctions), the spin-conserving collisions can be described in terms of the sum of the two relevant potentials ($V_{sum} = V_{A'} + V_{A''}$, the 'sum potential'), while the spin-changing

Elsevier Science B.V.
SSDI 0009-2614(95)00118-2

collisions are mainly controlled by the difference between the two potentials ($V_{diff} = V_{A'} - V_{A''}$, the 'difference potential') [11,23]. Using a new PES for this system, Alexander has recently achieved very good agreement with the available differential and integral cross sections obtained at center-of-mass (c.m.) collision energies of up to 442 cm^{-1} [12].

When the collision partner is a molecule the situation becomes more complicated; nonplanar geometries become possible and the anisotropy in the PES may depend sensitively on the direction of approach. In addition, long-range attractive interactions may increase in importance, and in radical–molecule collisions reactive pathways may be involved. In the latter case the inelastic collision outcome may be intimately linked to the reactive pathway, both having sampled the attractive well of the PES. If a long-lived collision complex is formed, a statistical approach may be more fruitful, since the interaction may be viewed as the reverse of the corresponding unimolecular reaction. For example, the inelastic collision of CH_2 with CO may yield information relevant to exit-channel interactions in the unimolecular reaction of ketene [24]. Thus, comparisons of the inelastic collisions of radicals with reactive and nonreactive colliders may yield important dynamical insights.

In the course of a series of investigations of the collision-induced dissociation (CID) of NO_2 in supersonic molecular beams [25], we observed inelastic collisions involving contaminant NO in the beam. A notable result was the dependence of the spin–orbit ratios in the excited $NO(^2\Pi_\Omega)$ on the nature of the collider, which stood in contrast to the rotational and Λ-doublet distributions that did not exhibit such pronounced dependence. These results have relevance to recent measurements in the upper atmosphere that revealed non-equilibrium spin–orbit ratios in $NO(^2\Pi_\Omega)$ under collisional conditions [26]. In this Letter, we summarize our observations on the fine-structure and rotational excitations in the inelastic collisions of NO, with particular emphasis on spin–orbit distributions, and discuss possible sources for the spin–orbit preferences observed in single collisions with molecular beams of Ar, Xe, CO, N_2, O_2, N_2O, and CO_2.

2. Experimental

The experiments are performed in a crossed molecular beams apparatus in which the two beams are differentially pumped and skimmed [25]. The pulsed (≈ 150 μs) molecular beams travel approximately 5 cm from the skimmer (2.9 mm diameter) to the center of the chamber and intersect at 90°, creating an overlap region of ≈ 1 cm^3. The first beam consists of $\leqslant 1\%$ NO seeded in 1.5 atm carrier gas

Table 1
Rotational temperatures and spin–orbit ratios obtained in the inelastic scattering of $NO(^2\Pi_\Omega)$

Collider	E_{col} (cm^{-1})	Rot. temperature (cm^{-1})		Spin–orbit ratio			
		$^2\Pi_{1/2}$	$^2\Pi_{3/2}$	exp.		calc.	
				restricted-sum method [a]	Boltzmann-fit method [b]	equilibrated [c]	statistical [d]
Ar	500 [e]	100 ± 2	111 ± 6	0.17 ± 0.01	0.18 ± 0.02	0.31	0.75
	2250 [f]	394 ± 20	256 ± 11	0.40 ± 0.02	0.39 ± 0.05	0.68	0.94
Xe	3000 [f]	367 ± 10	299 ± 8	0.63 ± 0.05	0.64 ± 0.05	0.69	0.96
CO	2050 [f]	262 ± 13	219 ± 12	0.64 ± 0.04	0.73 ± 0.12	0.60	0.94
N_2	2050 [f]	345 ± 8	281 ± 6	0.64 ± 0.03	0.71 ± 0.05	0.68	0.94
O_2	2150 [f]	262 ± 9	240 ± 12	0.49 ± 0.03	0.53 ± 0.07	0.61	0.94
N_2O	2400 [f]	333 ± 10	305 ± 13	0.51 ± 0.02	0.54 ± 0.06	0.68	0.95
CO_2	2400 [f]	380 ± 40	310 ± 30	0.39 ± 0.03	0.41 ± 0.05	0.70	0.95

[a] Obtained by the restricted-sum method (Eq. (2)). See text for details.
[b] Obtained from least-squares fits of the data to a Boltzmann distribution (Eq. (3) and (4)).
[c] Obtained assuming equality of the rotational and spin–orbit 'temperatures'.
[d] Defined by the total degeneracies (energetically accessible phase-space volumes) of each spin–orbit state. See text for details.
[e] Obtained by seeding NO in Ar. [f] Obtained by seeding NO in He.

(He or Ar for the NO + Ar scattering experiments, He for all the others), and the second beam is neat collider gas (Ar, Xe, CO, N_2, O_2, N_2O, and CO_2) at 1.5 atm backing pressure. The center-of-mass (c.m.) collision energies for the different collisional systems, as estimated for fully expanded seeded beams [25], are summarized in Table 1. The vacuum chamber base pressure is $\approx 2 \times 10^{-7}$ Torr, and under typical operating conditions (10 Hz pulse repetition rate) the pressure in the collision chamber is $< 2 \times 10^{-5}$ Torr. A rough estimate of the mean-free-path of the NO molecules in the collision region, obtained by considering the expected number densities in the supersonic molecular beams, indicates that these experiments are performed under nearly single-collision conditions.

The frequency-doubled output of an excimer-laser pumped dye-laser system is used for NO detection. The probe beam (225–227 nm; 15 ns duration; $\approx$ 150 μJ), which propagates in the plane of the molecular beams, is loosely focused with a 1 m focal-length lens to approximately 1 mm diameter and intersects the NO and the collider beams at the center of the collision region at 45° and 135°, respectively. NO is detected state-selectively by resonant multiphoton ionization (REMPI) via the $A\,^2\Sigma^+ \leftarrow X\,^2\Pi$ transition. The NO^+ ions are detected mass-selectively by a microchannel plate detector located at the end of a Wiley–McLaren time-of-flight (TOF) spectrometer which is mounted above the center of the collision chamber, perpendicularly to the plane of the molecular and laser beams. Due to poor Frank–Condon overlap, the ionization cross section of the A state of NO at 226 nm is much smaller than that for the $A\,^2\Sigma^+ \leftarrow X\,^2\Pi$ transition. The NO product state distributions are extracted from the REMPI spectra by assuming that the A ← X transitions are totally saturated (see Ref. [25] and references therein). No corrections for flux/density transformations have been attempted since the differences in the laboratory velocities of the detected NO(Ω, J) products are relatively small (except when seeding in Ar), due to the high velocity of the NO molecular beam. Data processing includes signal averaging (typically 10 shots per laser grating step) and shot-to-shot normalization of the signals using a photodiode to monitor the laser pulse energy.

To account for the rotational distributions of the unscattered NO, the collider pulsed valve is operated in an *on/off* mode. With no collisions, only the 2–3 lowest rotational states of NO($^2\Pi_{1/2}$; $v = 0$) have significant populations in the supersonic beam, corresponding to a temperature $\leqslant 5$ K. Although a small high-temperature tail is always present in the jet-cooled NO, the resulting populations of high rotational levels of NO (i.e. $J > 3.5$) are negligible compared to the low-J populations and the scattered NO signal [15]. Subtracting the NO signal obtained with the collider nozzle *off* (no collisions) yielded the collision-induced signal for $J > 3.5$. In general, the observed collision-induced signal for a monitored NO quantum state f is

$$P(\mathrm{f}) \propto \sum_{\mathrm{i} \neq \mathrm{f}} P_0(\mathrm{i})\,\sigma(\mathrm{f} \leftarrow \mathrm{i}) - \sum_{\mathrm{i} \neq \mathrm{f}} P_0(\mathrm{f})\,\sigma(\mathrm{i} \leftarrow \mathrm{f}), \quad (1)$$

where P_0(i) is the initial NO distribution, σ is the state-to-state inelastic cross section, and i, f denote an array of the quantum numbers sufficient to fully describe the experimentally resolved quantum states of NO (i.e. i, f = v, J, Ω, etc.). In these experiments, we are concerned with the multiplet (Ω = 1/2, 3/2) changing or conserving transitions and the rotationally (J) inelastic transitions. The first summation in Eq. (1) corresponds to scattering *into* the monitored quantum state of NO, while the second summation describes the reverse process. For rotational states $J > 3.5$, whose populations can be neglected in the supersonically cooled NO, the second summation in Eq. (1) is negligible; the collision-induced signal is due solely to scattering *into* these J-states and is given by a convolution of the inelastic scattering cross sections for transitions originating from the few initially populated low-J states of NO. For instance, at $T = 5$ K, the initial NO($^2\Pi_{1/2}$) rotational population ratios are (J = 0.5):(J = 1.5):(J = 2.5) $\approx$ 1 : 0.47 : 0.06, and thus the observed NO product state distributions P(f) reflect mainly inelastic scattering cross sections out of the two lowest NO J-states. For $J < 3.5$, the resulting collision-induced signal is a combination of two competing processes: scattering *into* and *out* of the particular NO state. For this reason, only the populations of NO with $J \geqslant 4.5$ were analyzed in this study.

3. Results and discussion

The scattered NO $^2\Pi_{1/2}$ and $^2\Pi_{3/2}$ rotational distributions obtained by scanning the laser over the NO (A ← X) transition are shown in Fig. 1. Since the results were analyzed assuming total saturation, only the integrated line intensities of the strongest transitions are used, i.e. the $R_{11} + Q_{21}$ and $Q_{11} + P_{21}$ branches for the $^2\Pi_{1/2}$ manifold and the $Q_{22} + R_{12}$ and $P_{22} + Q_{12}$ branches for the $^2\Pi_{3/2}$ manifold. In all the scattering experiments (except with Ar), no significant preference in the population of the Λ-doublet components is observed. For scattering by Ar at high collision energy, there appears to be a

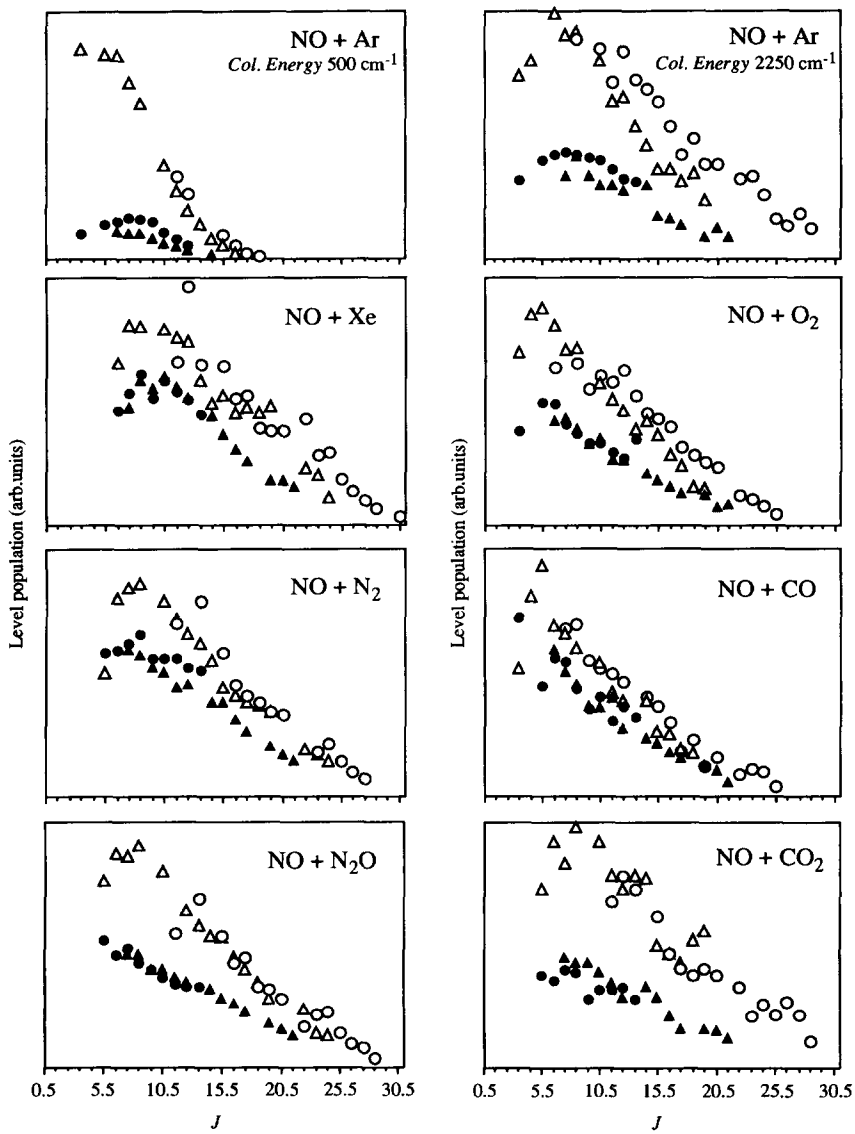

Fig. 1. NO($^2\Pi_{1/2}$ and $^2\Pi_{3/2}$) rotational level distributions obtained in the inelastic scattering of jet-cooled NO at collisional energies listed in Table 1. Scattering of NO by Ar is carried out at two different collisional energies obtained by seeding NO in He or Ar. The populations of the $\Pi(A')$ and $\Pi(A')$ Λ-doublet components are obtained from the Q and P/R branch lines of the NO (A ← X) transition, respectively. (△) $R_{11} + Q_{21}$, (○) $Q_{11} + P_{21}$, (▲) $P_{22} + Q_{12}$, (●) $Q_{22} + R_{12}$.

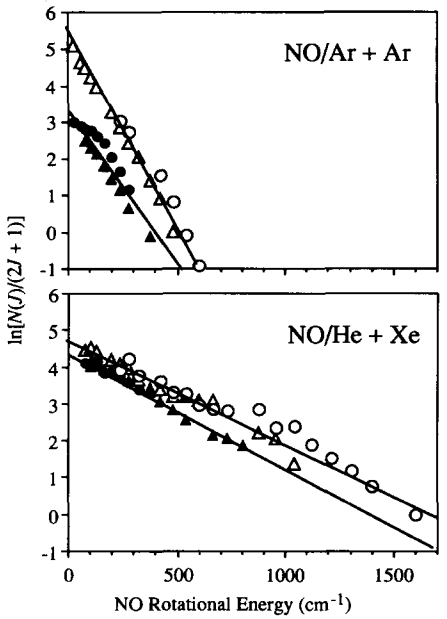

Fig. 2. Boltzmann plots of the NO($^2\Pi_\Omega$) rotational distributions obtained in the inelastic scattering of jet-cooled NO. The temperatures given in Table 1 are obtained from the slopes of the shown straight lines through the data.

preference for the $\Pi(A'')$ Λ-doublet component (see Fig. 1). Although the observed preference (up to 50% for some rotational levels) exceeds the statistical error bars ($\pm 10\%$–20%), it should be viewed with caution, since the possibility of incomplete saturation of the NO ($A \leftarrow X$) transition cannot be completely ruled out. We note however, that such preference is predicted theoretically [12].

Fig. 2 gives two examples of Boltzmann plots (i.e. log(intensity) versus rotational energy) of the scattered NO distributions. Shown are the distributions obtained for the NO(Ar seeded) + Ar and NO(He seeded) + Xe collisional systems. The rotational distributions for both NO spin–orbit states appear Boltzmann-like, as in all other experiments, justifying the use of rotational temperatures as a parameter characterizing the average rotational energy (see Table 1). The Boltzmann-like nature of the rotational distributions is in accordance with the exponential energy gap law often used to describe energy transfer in adiabatic collisions [2–4], which states that the probability of energy transfer from translational to internal degrees of freedom decreases exponentially with increasing amount of transferred energy. The rotational temperature thus provides a measure of the average energy transferred per collision. As seen from Table 1, the degree of rotational excitation generally increases with increasing collision energy. In most cases, the $^2\Pi_{3/2}$ and $^2\Pi_{1/2}$ rotational temperatures are fairly close, although the former tends to be consistently colder.

The rotational distribution and the spin–orbit ratio obtained in our NO + Ar scattering experiment at 500 cm^{-1} c.m. collision energy agree with earlier results at similar collision energy [15]. However, our results do not reveal the even–odd oscillations in the multiplet-conserving cross sections as a function of J observed in the earlier work. In that work, the oscillations were ascribed to quantum interference between scattering from the opposite ends of an almost homonuclear NO molecule resulting in more favorable cross sections for the even ΔJ transitions for low rotational states [15]. The absence of such oscillations in our data (within our signal/noise ratio) is probably due to the higher NO beam temperature in our experiment, resulting in significant initial population of NO ($J = 1.5$) (see Section 2). Averaging of the oscillatory populations originating from scattering of the $J = 0.5$ and 1.5 states, one of which favors even and the other one odd product rotational states, averages out the oscillations in the individual distributions.

Due to overlap and weak signal levels, not all the rotational levels are monitored in our experiments, complicating the extraction of the scattered NO spin–orbit ratios. We have used two methods in analyzing the data. In the first method, only the populations of rotational levels available in both the $^2\Pi_{3/2}$ and $^2\Pi_{1/2}$ manifolds were summed, and their ratio was used as an approximation to the true NO spin–orbit ratio, i.e.

$$\frac{\Pi_{3/2}}{\Pi_{1/2}} = \frac{\Sigma_N P(\Omega = 3/2, N)}{\Sigma_N P(\Omega = 1/2, N)}, \qquad (2)$$

where the summation is restricted to a set of the NO N-levels ($N = J - 1/2$ and $J - 3/2$ for $^2\Pi_{1/2}$ and $^2\Pi_{3/2}$, respectively) for which experimental data are available for both spin–orbit manifolds (typically, $J = 5.5$–20.5).

In view of the Boltzmann-like nature of all the scattered NO rotational distributions, the spin–orbit ratios can also be extracted from least-squares fits of the form

$$P_{\Omega}(J) = A_{\Omega}(2J+1)\exp\left(-\frac{E_{\mathrm{rot}}(J)}{\theta_{\Omega}}\right),$$

$$\Omega = 1/2,\ 3/2 \qquad (3)$$

where $E_{\mathrm{rot}}(J)$ is the NO rotational energy, and A_{Ω} and θ_{Ω} (i.e. the rotational temperature) are the fitting parameters. The spin–orbit ratio is then given by [25]

$$\frac{^2\Pi_{3/2}}{^2\Pi_{1/2}} = \frac{A_{3/2}\theta_{3/2}}{A_{1/2}\theta_{1/2}}. \qquad (4)$$

This approach offers the advantage of not requiring summation of the populations of *all* rotational states, some of which are missing in the experimental distributions. However, it assumes arbitrarily that all the rotational levels can be fit by a single temperature parameter.

The spin–orbit ratios obtained by the restricted-sum (Eq. (2)) and Boltzmann-fit (Eqs. (3), (4)) methods are listed in Table 1. Notice that the spin–orbit ratios obtained by the two methods are not always identical, reflecting the differences in the data analysis methods. Nevertheless, the relative values of the spin–orbit ratios derived from these methods for the various colliders are similar, and thus provide insights into trends in the scattered NO spin–orbit ratios.

Since the NO($^2\Pi_{3/2}$) population in the expanded molecular beam is negligible, the NO($^2\Pi_{1/2}$) and NO($^2\Pi_{3/2}$) distributions reflect the inelastic cross sections for the multiplet-conserving and multiplet-changing transitions, respectively. The relative magnitude of the cross sections for multiplet-changing transitions, quantified by the spin–orbit ratio, is affected markedly by the nature of the collider. Since this value is also sensitive to the collision energy (as shown in Table 1 for collisions with Ar), criteria for comparing the spin–orbit ratios obtained with different colliders are needed. Two such guidelines are used here. Within the framework of a thermal approach, we define the propensity for spin–orbit excitation by comparing the rotational and spin–orbit excitations for each collider. When the spin–orbit and rotational temperatures are equal, they are considered 'equilibrated'. The second guideline defines a 'statistical' NO spin–orbit ratio by the total number of energetically accessible quantum levels (the accessible phase-space volume) within each of the two spin–orbit states. The statistical values of the spin–orbit ratios approach their degeneracy ratio of 1 when the collision energy is much larger than the NO spin–orbit energy separation of 123 cm^{-1}. The 'equilibrated' and 'statistical' spin–orbit ratios obtained using the above criteria are also listed in Table 1.

Table 1 shows that the scattered NO spin–orbit ratios are always smaller than 'statistical'. The agreement with the 'equilibrated' values is generally better, despite the marked dependence of the observed spin–orbit ratios on the collider. We note that Ar, O_2, CO_2, and N_2O result in spin–orbit distributions that are relatively 'cold' compared to the corresponding rotational excitations, while Xe, CO, and N_2 produce NO spin–orbit ratios that are close to (or even slightly larger than) those expected in the case of electronic–rotational equilibrium.

The multiplet-changing scattering events resulting in population of the NO($^2\Pi_{3/2}$) state involve two intermolecular electronic potential energy surfaces. In previous theoretical studies, it has been shown that for collisions of a closed-shell atom and a $^2\Pi$ molecule belonging to Hund's case (a), the multiplet-conserving transitions are governed by the average potential (V_{sum}), while the multiplet-changing transitions are governed by the difference potential (V_{diff}) [11,23,27]. Thus, in this case, the product spin–orbit ratios reflect the strength of V_{diff}. However, when the collisionally excited NO belongs to intermediate Hund's cases (a) and (b), as it is in the present case where most of the excited NO is in $J > 10.5$, this simple description fails. Instead, the population of each spin–orbit state depends on both V_{sum} and V_{diff}, and the population of each NO(J, Λ, Ω) state is modified by the interference between the two pathways. Thus, a theoretical description in this case is complicated, especially for polyatomic colliders.

Another intriguing question relevant to polyatomic colliders involves the participation of long-range forces in cases where the interaction can be

attractive. For the NO–Ar system, the largest V_{diff} is localized in the short-range region near the classical turning point [12,19], and it is currently accepted that the short-range potential is the most important in governing the scattering events [7]. The possible importance of long-range attraction in the case of polyatomic colliders can be examined by comparing isoelectronic colliders (e.g., CO and N_2 or CO_2 and N_2O).

The structure of van der Waals complexes of NO was determined only with very few colliders. For example, in the case of inert colliders such as Ar, a perpendicular geometry is favored [28,29]. For the other colliders studied here, the geometries have not been determined. Comparing CO and N_2, chemical and electronic structure considerations would favor larger long-range attraction for the former, at least in a restricted set of geometries; however, the observed NO spin–orbit excitations produced by these two molecules are very similar. Larger anisotropy and possibly long-range attraction is also expected in the collisions of NO with N_2O than with CO_2. While the observed spin–orbit excitations seem to reflect this expectation, the difference can also be attributed to short-range, impulsive interactions. Finally, the assumption of the importance of long-range interactions in inelastic scattering of NO fails to explain the result obtained with O_2. Among all the studied colliders, this is the molecule for which significant attractive interaction with NO is expected. We find, however, that the spin–orbit excitation observed in the O_2–NO system is colder than the one obtained with N_2 and CO, suggesting again that the long-range part of the PES does not have significant effect in these systems. We also note that in the inelastic scattering of OH with CO and N_2, similar spin–orbit excitations are obtained despite the much more attractive HOCO PES [30].

Thus, no indication of the importance of long-range attractions has been obtained in the cases studied here at c.m. collision energies of 2000–3000 cm^{-1}, and consequently a simple, chemically intuitive approach cannot be used to explain our results. A small influence of long-range forces and large impact parameter collisions may be better revealed in differential (angle-resolved) scattering measurements.

In conclusion, the spin–orbit ratios obtained in the inelastic collision of NO with a series of monatomic, diatomic and triatomic colliders depend on the nature of the collider, while the population of the Λ-doublet components is equal, with the possible exception of Ar. The spin–orbit ratios are generally different than those calculated based on statistical equilibrium with the rotational temperature, and are always colder than the ratios expected based on degeneracies alone. Following excitation, the NO fragment is best described as an intermediate Hund's case (a) and (b), and no simple propensity rules for the spin–orbit ratios can be obtained by analogy with collisions of NO with Ar. However, it is likely that the spin–orbit ratios are mainly governed by the short-range repulsive part of the PES, even in cases where attractive interactions are possible. As in the collisions of OH with CO and N_2, no indication of the influence of the attractive part of the potential is evident. Measurements of differential cross sections may be better able to unravel small contributions from large impact-parameter collisions. It would also be interesting to compare our results to radical–radical inelastic collisions in which attractive interactions are more likely to dominate.

Acknowledgement

The authors wish to thank Millard Alexander for fruitful discussions. The research is supported by DOE grant No. DE-FG03-88ER13959.

References

[1] K. Liu, R.G. Macdonald and A.F. Wagner, Intern. Rev. Phys. Chem. 9 (1990) 187.
[2] J. Troe, J. Chem. Phys. 66 (1977) 4745.
[3] J.T. Yardley, Introduction to molecular energy transfer (Academic Press, New York, 1980).
[4] H. Hippler and J. Troe, in: Advances in gas-phase photochemistry and kinematics: bimolecular collisions, eds. M.N.R. Ashfold and J.E. Baggott (The Royal Society of Chemistry, London, 1989) pp. 209–262.
[5] D.J. Krajnovich, K.W. Butz, H. Du and C.S. Parmenter, J. Chem. Phys. 91 (1989) 7705, 7725.
[6] Z. Ma, S.D. Jons, C.F. Giese and W.R. Gentry, J. Chem. Phys. 94 (1991) 8608.
[7] R.G. Macdonald and K. Liu, J. Chem. Phys. 93 (1990) 2431; 97 (1992) 978.

[8] H. Meyer, J. Chem. Phys. 101 (1994) 6686, 6697.
[9] S. Green and R.N. Zare, Chem. Phys. 7 (1975) 62.
[10] R.N. Dixon and D. Field, Proc. Roy. Soc. Ser. A 368 (1979) 99.
[11] M.H. Alexander, J. Chem. Phys. 76 (1982) 5974.
[12] M.H. Alexander, J. Chem. Phys. 99 (1993) 7725, and references therein.
[13] M.H. Alexander and B. Pouilly, J. Chem. Phys. 79 (1983) 1545.
[14] P. Andresen, D. Häusler and H.W. Lülf, J. Chem. Phys. 81 (1984) 571.
[15] H. Joswig, P. Andresen and R. Schinke, J. Chem. Phys. 85 (1986) 1904.
[16] P.J. Dagdigian, J. Chem. Phys. 90 (1989) 2617.
[17] P.J. Dagdigian, M.H. Alexander and K. Liu, J. Chem. Phys. 91 (1989) 839.
[18] S.M. Ball, G. Hancock and M.R. Heal, J. Chem. Soc. Faraday Trans. 90 (1994) 1467.
[19] G.C. Nielson, G.A. Parker and R.T Pack, J. Chem. Phys. 66 (1977) 1396.
[20] P. Andresen, H. Joswig, H. Pauly and R. Schinke, J. Chem. Phys. 77 (1982) 2204.
[21] S.D. Jons, J.F. Shirley, M.T. Vonk, C.F. Giese and W.R. Gentry, J. Chem. Phys. 97 (1992) 7831.
[22] A.G. Suits, L.S. Bontuyan, P.L. Houston and B.J. Whitaker, J. Chem. Phys. 96 (1992) 8618;
L.S. Bontuyan, A.G. Suits, P.L. Houston and B.J. Whitaker, J. Chem. Phys. 97 (1993) 6342.
[23] M.H. Alexander, Chem. Phys. 92 (1985) 337.
[24] W.H. Green Jr., C.B. Moore and W.F. Polik, Ann. Rev. Phys. Chem. 43 (1992) 307.
[25] A. Sanov, C.R. Bieler and H. Reisler, J. Phys. Chem., in press.
[26] W.A.M. Blumberg, private communication.
[27] M.H. Alexander, J. Chem. Phys. 80 (1984) 4325.
[28] B.J. Howard, C.M. Western and P.D. Mills, Faraday Discussions Chem. Soc. 73 (1982) 129.
[29] C.M. Western and B.J. Howard, J. Phys. Chem. 90 (1986) 4961.
[30] D.M. Sonnenfroh, R.G. Macdonald and K. Liu, J. Chem. Phys. 94 (1991) 6508.